ACS APPLIED MATERIALS & INTERFACES
Letter
www.acsami.org

CdSe Nanowire-Based Flexible Devices: Schottky Diodes, Metal–Semiconductor Field-Effect Transistors, and Inverters

Weifeng Jin,[†] Kun Zhang,[†] Zhiwei Gao,[†] Yanping Li,[†] Li Yao,[†] Yilun Wang,[†] and Lun Dai*,[†,‡]

[†]State Key Lab for Mesoscopic Physics and School of Physics, Peking University, Beijing 100871, China
[‡]Collaborative Innovation Center of Quantum Matter, Beijing 100871, China

Supporting Information

ABSTRACT: Novel CdSe nanowire (NW)-based flexible devices, including Schottky diodes, metal–semiconductor field-effect transistors (MESFETs), and inverters, have been fabricated and investigated. The turn-on voltage of a typical Schottky diode is about 0.7 V, and the rectification ratio is larger than 1×10^7. The threshold voltage, on/off current ratio, subthreshold swing, and peak transconductance of a typical MESFET are about −0.3 V, 4×10^5, 78 mV/dec, and 2.7 μS, respectively. The inverter, constructed with two MESFETs, exhibits clear inverting behavior with the gain to be about 28, 34, and 38, at the supply voltages (V_{DD}) of 3, 5, and 7 V, respectively. The inverter also shows good dynamic behavior. The rising and falling times of the output signals are about 0.18 and 0.09 ms, respectively, under 1000 Hz square wave signals input. The performances of the flexible devices are stable and reliable under different bending conditions. Our work demonstrates these flexible NW-based Schottky diodes, MESFETs, and inverters are promising candidate components for future portable transparent nanoelectronic devices.

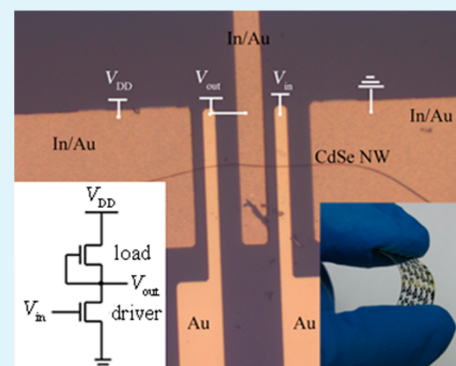

KEYWORDS: *flexible, nanowires, Schottky diodes, MESFETs, inverters*

During the past decade, flexible devices have attracted enormous attention both in industry and academic fields for their potential application in developing low-cost and wearable electronic/optoelectronic products. Up to date, most flexible devices are based on organic semiconductors.[1−3] Compared to organic semiconductors, inorganic semiconductors possess more superior electrical performance and stability, and are more compatible with present microelectronic technology. However, traditional bulk and thin film inorganic semiconductors are fragile under external strain, which restricts their application in flexible devices. How to apply inorganic semiconductors to flexible devices is attracting more and more attention in the past few years.[4−6]

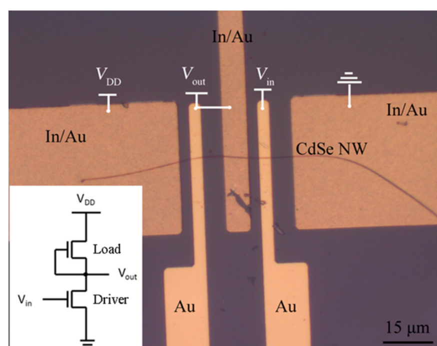

Figure 1. Optical image of an as-fabricated Schottky diodes, MESFETs, and inverter on a PET substrate. The white lines show the way the circuit is connected during the inverter measurement. The inset: corresponding circuit diagram of the inverter.

Single-crystalline inorganic semiconductor nanowires (NWs) have advantage over their bulk or thin film counterparts in mechanical flexibility,[7−9] which makes them more suitable for the application in flexible devices. In the past few years, various inorganic semiconductor NWs based flexible devices have been reported, including photodetectors, stress sensors, supercapacitances, lithium ion batteries and solar cells, etc.[10−15] Diodes, field-effect transistors (FETs), and inverters are basic components of modern integrated circuits. So far, only few works about these devices made of inorganic NWs on flexible substrates were reported.[16−18] Compared to metal-oxide-semiconductor FETs (MOSFETs), metal–semiconductor FETs (MESFETs) have the advantage of larger gate capacitance coupling, and simpler fabrication process.[19−22] Furthermore, traditional gate dielectrics (SiO_2, HfO_2, Al_2O_3, etc.) used in MOSFETs are fragile, which hinders the application of MOSFETs in flexible devices. Rogers et al. reported flexible inverters constructed with MESFETs based on printed arrays of aligned GaAs microwires. The GaAs microwire arrays were fabricated by the "top-down" etching

Received: April 3, 2015
Accepted: June 10, 2015
Published: June 10, 2015

© 2015 American Chemical Society

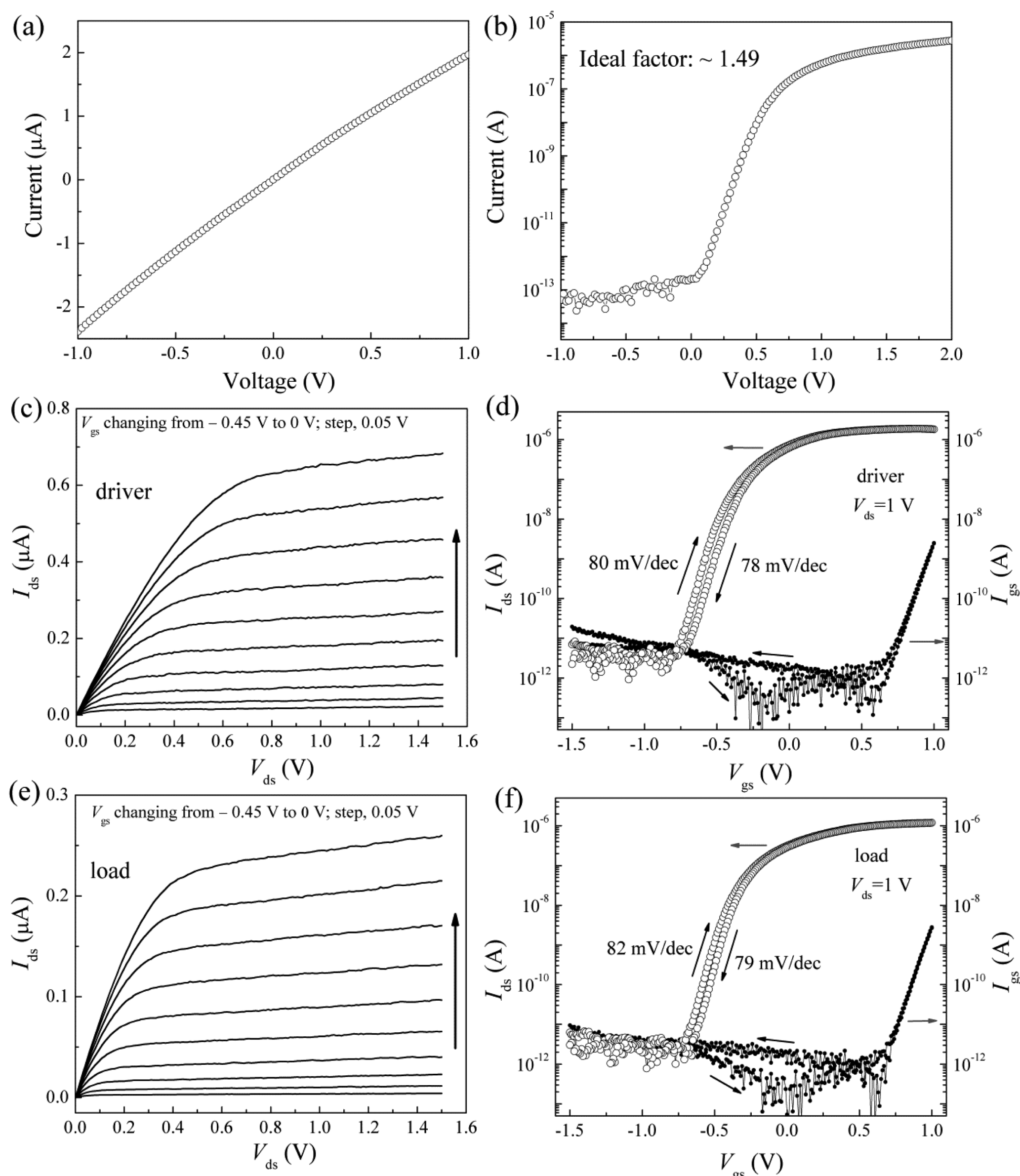

Figure 2. (a) Typical $I-V$ curve measured between any two neighboring In/Au electrodes. (b) Typical $I-V$ curve measured between any neighboring Au and In/Au electrodes. (c) The $I_{ds}-V_{ds}$ curves of the driver MESFET at various V_{gs}. The V_{gs} changes from −0.45 to 0 V, with a step of 0.05 V, and (d) the corresponding gate transfer characteristic curves (hollow circles) and the gate leakage curves (solid circles) under double sweeping of V_{gs}. The arrows indicate the sweeping directions. (e) The $I_{ds}-V_{ds}$ curves of the load MESFET at various V_{gs}. The V_{gs} changes from −0.45 to 0 V, with a step of 0.05 V, and (f) the corresponding gate transfer characteristic curves (hollow circles) and the gate leakage curves (solid circles) of the load MESFET under double sweeping of V_{gs}.

method. The maximum voltage gain is only 1.52 at the supply voltage (V_{DD}) of 5 V.[17]

In this work, we fabricated high-performance CdSe NW-based flexible devices with the "bottom up" method, including Schottky diodes, MESFETs, and inverters. The turn-on voltage of a typical Schottky diode is about 0.7 V, and the rectification ratio is larger than 1×10^7. The threshold voltage, on/off current ratio, subthreshold swing, and peak transconductance of a typical MESFET are about −0.3 V, 4×10^5, 78 mV/dec, and 2.7 μS, respectively. The inverter, constructed with two MESFETs, exhibits clear inverting behavior, with gain to be about 28, 34 and 38, respectively, at V_{DD} = 3, 5, and 7 V. The inverter also shows good dynamic behavior. Under 1000 Hz square wave signals input, the rising and falling times of the output signals are about 0.18 and 0.09 ms, respectively. These devices are reliable and stable under different bending conditions. The as-fabricated NW-based flexible Schottky diodes, MESFETs, and inverters promise a potential application in future portable transparent nanoelectronic field.

The In doped single-crystalline n-type CdSe NWs were synthesized via the low pressure chemical vapor deposition (CVD) method.[23] The fabrication process of the flexible devices was as follows: First, we dispersed the CdSe NWs in ethanol with an ultrasonic process, and then dropped the CdSe NW suspension onto a polyethylene terephthalate (PET) substrate. After that, we fabricated three ohmic contact In/Au (20/150 nm) electrodes and two Schottky contact Au (150 nm) electrodes in succession onto a single CdSe NW, using UV lithography, thermal evaporation, and lift-off process. The Au electrodes were placed in between the In/Au electrodes. The

DOI: 10.1021/acsami.5b02929
ACS Appl. Mater. Interfaces 2015, 7, 13131−13136

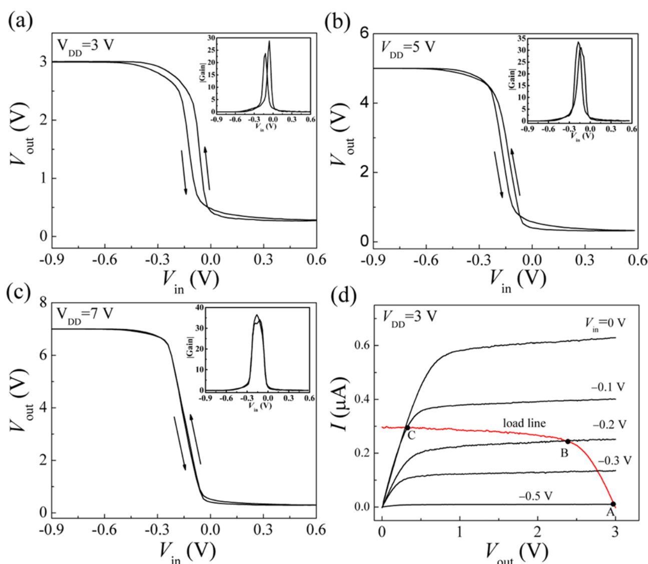

Figure 3. Static VTC curves of a typical inverter measured at (a) V_{DD} = 3 V, (b) V_{DD} = 5 V, and (c) V_{DD} = 7 V. The arrows indicate the sweeping directions of V_{in}. The insets: the voltage gain curves obtained from the corresponding VTC curves. (d) Graphical determination of the static VTC for the inverter at V_{DD} = 3 V.

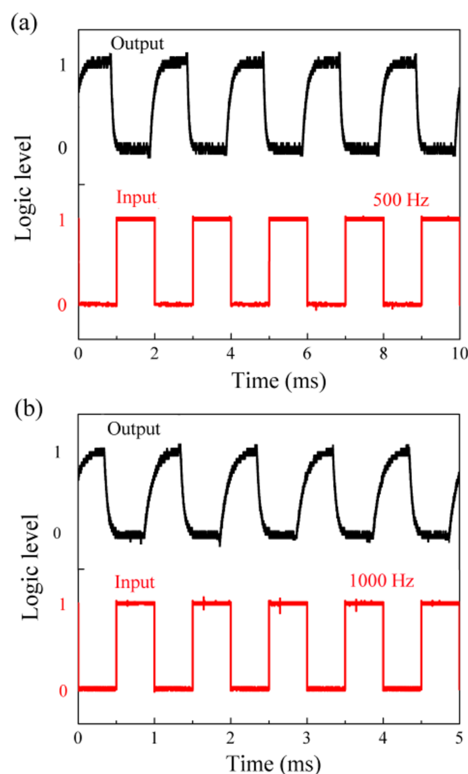

Figure 4. Dynamic behaviors (dark curves) of the inverter measured at V_{DD} = 3 V, with (a) 500 Hz, (b) 1000 Hz square wave signals input (red curves).

static electrical measurement was done with a semiconductor characterization system (Keithley 4200). The dynamic behavior of the inverters was investigated with a digital oscilloscope (Tektronix DPO 2024) and an arbitrary waveform generator (Tektronix AFG3000). All the measurements were done at room temperature in darkness.

Figure 1 shows the optical image of an as-fabricated Schottky diodes, MESFETs, and inverter on a PET substrate. The Schottky diodes formed between any neighboring In/Au electrode and Au electrode. For a single MESFET, two In/Au electrodes acted as the source and drain, and the Au electrode in between them acted as the gate. For the inverter, one MESFET acted as the driver, and the other acted as the load. The white lines show how the circuit is connected during the inverter measurement. Corresponding circuit diagram is plotted in the inset.

We first evaluated the ohmic contact behavior of the In/Au electrodes, and the Schottky contact behavior of the Au electrodes, when contacting to the CdSe NW. Typical $I-V$ curve measured between any two neighboring In/Au electrodes is shown in Figure 2a. The linear behavior indicates the ohmic contact behavior of the In/Au electrodes. Typical $I-V$ curve measured between any neighboring Au and In/Au electrodes is shown in Figure 2b. The clear rectification characteristic verifies the good Schottky contact behavior of the Au electrodes. The turn-on voltage of the corresponding Schottky diode is about 0.7 V, and the rectification ratio is larger than 1×10^7 measured between −1 and 2 V. We can obtain the diode ideality factor (n) to be about 1.49, by curve fitting with the thermionic emission theory based equation $I = I_0[\exp(eV/nkT) - 1]$, where I_0 is the reverse saturation current, e is the electron charge, V is the applied bias, k is the Boltzmann constant, and T is the absolute temperature.[24] Figure 2c shows the drain-source current (I_{ds}) versus drain−source voltage (V_{ds}) relation of the driver MESFET at various gate−source voltage (V_{gs}). It can be seen that the Schottky contact gate has an effective modulation on the CdSe NW channel. At identical V_{ds}, I_{ds} increases with V_{gs}, showing the n-type conductance characteristic of the CdSe NW. Figure 2d shows the corresponding gate transfer characteristic curves and the gate leakage curves (V_{ds} = 1 V) under double sweeping of V_{gs}. The arrows indicate the sweeping directions. The hysteresis of I_{ds} is small (∼40 mV), suggesting the amount of related trapping states and/or mobile charges at the Au/CdSe NW interface be small. The on/off current ratio and subthreshold swing ($S = \mathrm{In}10[\mathrm{d}V_{gs}/\mathrm{d}(\mathrm{In}I_{ds})]$) are about 4×10^5 and 78 mV/dec, respectively. The threshold voltage is about −0.3 V, determined from the intersection point of the exponential and nonexponential region of the MESFET transfer characteristic curve.[25] The transconductance ($g_m = \mathrm{d}I_{ds}/\mathrm{d}V_{gs}$) has a peak value of about 2.7 μS. The gate leakage (I_{gs}) is much smaller than on-state I_{ds} at identical V_{gs}. Figure 2e and f show, respectively, the output characteristic curves, and transfer characteristic curves together with the gate leakage curves of the driver MESFET. The threshold voltage, on/off current ratio, subthreshold swing, etc., are very close to those of the load MESFET. The electron concentration and field-effect mobility in the CdSe NWs can be estimated to be about 5.16×10^{17}/cm^3 and 517 cm^2/(V s), respectively (see the Supporting Information, Figure S1).

The static voltage transfer characteristic (VTC) curves of the typical inverter constructed on the above two MESFETS measured at V_{DD} = 3, 5, and 7 V, are shown in Figure 3a−c, respectively. The arrows indicate the sweeping directions of the input voltage (V_{in}). We can see that the inverter exhibits good inverting behavior. For V_{DD} = 3, 5, and 7 V, an input swing from −0.4 to 0.4 V can cause an output swing ($(V_{out})_{max} - (V_{out})_{min}$) to be larger than 91%, 93%, and 94% of V_{DD}, respectively. The corresponding voltage gain (= $-\mathrm{d}V_{out}/\mathrm{d}V_{in}$) curves are plotted in the insets of the corresponding figures.

DOI: 10.1021/acsami.5b02929
ACS Appl. Mater. Interfaces 2015, 7, 13131−13136

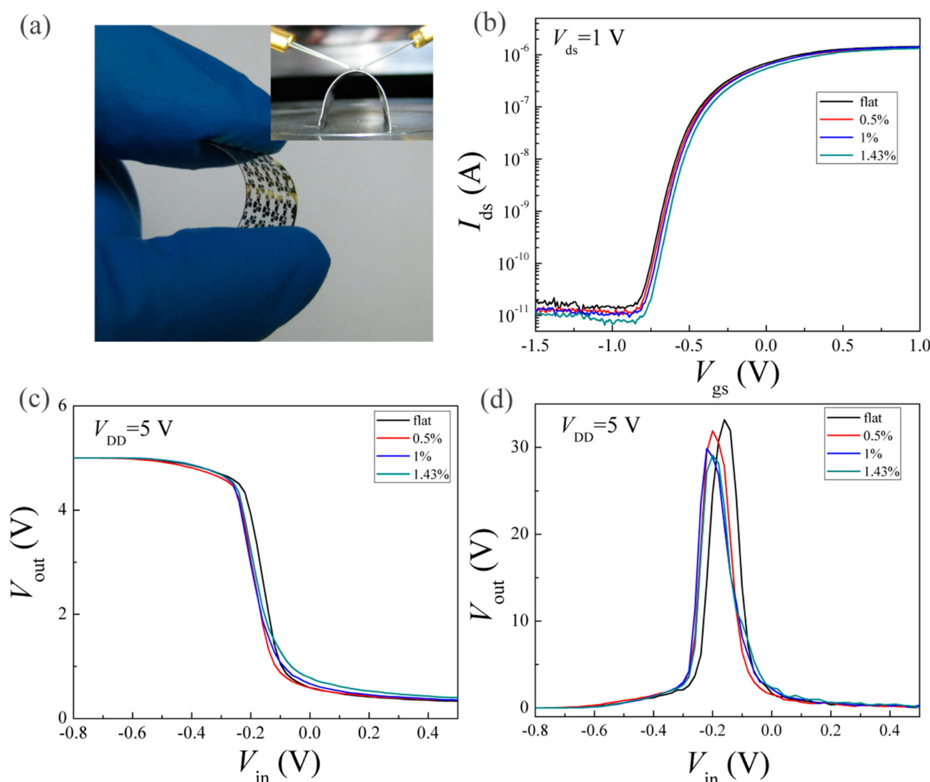

Figure 5. (a) Photographs of the devices under bending condition. (b) The gate transfer characteristic curves for the driver MESFET measured under flat condition and under a strain of 0.5%, 1%, and 1.43%. (c) VTC curves and (d) corresponding gain curves of the inverter measured under flat condition and under a strain of 0.5%, 1%, and 1.43%.

The maximum gain of the inverter are about 28, 34, and 38 for V_{DD} = 3, 5, and 7 V, respectively, much higher than the previously reported NW-based flexible inverters.[17,18] We have also done the statistical analysis on the performance of 12 as-fabricated devices. The maximum gain at V_{DD} = 5 V can be as high as 91 (see the Supporting Information, Figure S3).

The inverting behavior can be understood by analyzing the graphical determination of the static VTC for the inverter, as shown in Figure 3d. All the curves in Figure 3d are experimental results at V_{DD}= 3 V. The red line is the load line, which is the $I_{ds}-V_{ds}$ relation of the load MESFET at V_{gs} = 0 V, because the gate and source of the load are connected in the inverter. The dark lines are the $I_{ds}-V_{ds}$ (namely, V_{out}) relation of the driver MESFET at various V_{gs} (namely, V_{in}). Three intersections (marked A, B, and C points) of the red line and the dark lines reflect the actual operating points of the inverter, in which the channel currents for the driver and the load are identical. At point A, V_{in} is −0.5 V, the driver is nearly turned off. Therefore, the channel current is small, corresponding to a small V_{ds} for the load. Thus, V_{out} (=$V_{DD}-V_{ds}$ (load)) is very close to V_{DD}. As V_{in} increases, the driver MESFET tends to be turned on. Therefore, the channel current as well as the V_{ds} (load) increases, resulting a decrease of V_{out}. It is worth noting that when V_{in} increases from −0.2 to −0.1 V (corresponding to points B and C), V_{out} decreases sharply from 2.4 to 0.3 V, corresponding to a high gain of the inverter.

Figure 4a, b show the dynamic behavior of the inverter measured at V_{DD} = 3 V under 500 and 1000 Hz square wave signals input, respectively. At the input terminal, logic 0 and logic 1 correspond to −0.9 and 0.6 V, respectively. At the output terminal, logic 0 and logic 1 correspond to 0.27 and 3 V, respectively. Clear inversion behavior is observed. Under 1000 Hz signals input, although the output waveform exhibits kind of deterioration due to the RC delay, the rising (t_r) and falling times (t_f), obtained at 10% and 90% of the output values,[26] are about 0.18 and 0.09 ms, respectively. We attribute the good dynamic behavior of the inverter to the satisfying performance of the involved MESFETs, especially the small hysteresis. To the best of our knowledge, only few work about the dynamic behavior of NW-based flexible inverters was reported so far.[27]

We also evaluated the performance of the devices under bending conditions. Figure 5a is photographs of the devices under bending condition. For measurement purposes, we adhered the PET substrate to a bending tinplate with the channel direction along the circular arc of the bending region. The strain on the device can be modulated by changing the bending radium, based on the equation $\sigma = d/2r$,[5] in which σ is the strain, d is the thickness of PET substrate (110 μm), and r is the bending radium. Figure 5b shows the gate transfer characteristic curves for the driver MESFET measured under flat condition and under a strain of 0.5%, 1%, and 1.43%. We can see that the performance of the MESFET changes little under different bending conditions. The result for the load MESFET is similar. The VTC and the corresponding gain curves of the inverter measured under flat condition and under a strain of 0.5%, 1%, and 1.43%, are shown in Figures 5c, d, respectively. The maximum gain of the inverter under flat condition and under a strain of 0.5%, 1%, and 1.43%, are about 34, 32, 30, and 29, respectively. We attribute the good stability of the flexible MESFETs and inverters to the excellent mechanical flexibility of single-crystalline CdSe NWs. More than 12 devices have been tested under the same condition, and all of them exhibited good stability. Moreoever, the performance of the inverter was reproducible after more than 500

DOI: 10.1021/acsami.5b02929
ACS Appl. Mater. Interfaces 2015, 7, 13131−13136

bending cycles (see the Supporting Information, Figure S4), demonstrating the reliability of the flexible device. It is worth noting that the devices did not show obvious degeneration in performance after staying under air condition for more than 4 months.

In conclusion, flexible Schottky diodes, MESFETs, and inverters based on CdSe NWs have been fabricated and investigated for the first time. The turn-on voltage of a typical Schottky diode is about 0.7 V, and the rectification ratio is larger than 1×10^7. The threshold voltage, on/off current ratio, subthreshold swing, and peak transconductance of a typical MESFET are about −0.3 V, 4×10^5, 78 mV/dec, and 2.7 μS, respectively. The inverter, constructed with two MESFETs, exhibits clear inverting behavior, with the maximum gain to be about 28, 34, and 38 at V_{DD} = 3, 5, and 7 V, respectively. The inverter also shows good dynamic behavior. Under 1000 Hz square wave signals input, the rising and falling times of the output are about 0.18 and 0.09 ms, respectively. The performances of the devices are reliable and stable under different bending conditions. Our work demonstrated the potential application of the NW-based flexible Schottky diodes, MESFETs, and inverters in future portable transparent nanoelectronic field.

■ ASSOCIATED CONTENT

Ⓢ Supporting Information

Figures S1−S4. The Supporting Information is available free of charge on the ACS Publications website at DOI: 10.1021/acsami.5b02929.

■ AUTHOR INFORMATION

Corresponding Author

*E-mail: lundai@pku.edu.cn.

Notes

The authors declare no competing financial interest.

■ ACKNOWLEDGMENTS

This work was supported by the National Basic Research Program of China (2013CB921901 and 2012CB932703), and the National Natural Science Foundation of China (61125402, 51172004, 11474007, and 61404003).

■ REFERENCES

(1) Nyholm, L.; Nyström, G.; Mihranyan, A.; Strømme, M. Toward Flexible Polymer and Paper-Based Energy Storage Devices. *Adv. Mater.* **2011**, *23*, 3751−3769.

(2) Forrest, S. R. The Path to Ubiquitous and Low-Cost Organic Electronic Appliances on Plastic. *Nature* **2004**, *428*, 911−918.

(3) Lewis, J. Material Challenge for Flexible Organic Devices. *Mater. Today* **2006**, *9*, 38−45.

(4) Cao, Q.; Kim, H.-S.; Pimparkar, N.; Kulkarni, J. P.; Wang, C.; Shim, M.; Roy, K.; Alam, M. A.; Rogers, J. A. Medium-Scale Carbon Nanotube Thin-film Integrated Circuits on Flexible Plastic Substrates. *Nature* **2008**, *454*, 495−500.

(5) Kim, D.-H.; Ahn, J.-H.; Choi, W. M.; Kim, H.-S.; Kim, T.-H.; Song, J.; Huang, Y. Y.; Liu, Z.; Lu, C.; Rogers, J. A. Stretchable and Foldable Silicon Integrated Circuits. *Science* **2008**, *320*, 507−511.

(6) Ko, H. C.; Stoykovich, M. P.; Song, J.; Malyarchuk, V.; Choi, W. M.; Yu, C.-J.; Geddes Iii, J. B.; Xiao, J.; Wang, S.; Huang, Y.; Rogers, J. A. A Hemispherical Electronic Eye Camera based on Compressible Silicon Optoelectronics. *Nature* **2008**, *454*, 748−753.

(7) Wang, X.; Zhou, J.; Song, J.; Liu, J.; Xu, N.; Wang, Z. L. Piezoelectric Field Effect Transistor and Nanoforce Sensor Based on a Single ZnO Nanowire. *Nano Lett.* **2006**, *6*, 2768−2772.

(8) Zhou, Y. S.; Hinchet, R.; Yang, Y.; Ardila, G.; Songmuang, R.; Zhang, F.; Zhang, Y.; Han, W.; Pradel, K.; Montès, L.; Mouis, M.; Wang, Z. L. Nano-Newton Transverse Force Sensor Using a Vertical GaN Nanowire Based on the Piezotronic Effect. *Adv. Mater.* **2013**, *25*, 883−888.

(9) Liu, W.; Lee, M.; Ding, L.; Liu, J.; Wang, Z. L. Piezopotential Gated Nanowire-Nanotube Hybrid Field-Effect Transistor. *Nano Lett.* **2010**, *10*, 3084−3089.

(10) Chen, G.; Liu, Z.; Liang, B.; Yu, G.; Xie, Z.; Huang, H.; Liu, B.; Wang, X.; Chen, D.; Zhu, M.-Q.; Shen, G. Single-Crystalline p-Type Zn_3As_2 Nanowires for Field-Effect Transistors and Visible-Light Photodetectors on Rigid and Flexible Substrates. *Adv. Funct. Mater.* **2013**, *23*, 2681−2690.

(11) Wang, X.; Lu, X.; Liu, B.; Chen, D.; Tong, Y.; Shen, G. Flexible Energy-Storage Devices: Design Consideration and Recent Progress. *Adv. Mater.* **2014**, *26*, 4763−4782.

(12) Wang, X.; Liu, B.; Hou, X.; Wang, Q.; Li, W.; Chen, D.; Shen, G. Ultralong-Life and High-Rate Web-like $Li_4Ti_5O_{12}$ Anode for High-Performance Flexible Lithium-Ion Batteries. *Nano Res.* **2014**, *7*, 1073−1082.

(13) Yuan, H.-C.; Shin, J.; Qin, G.; Sun, L.; Bhattacharya, P.; Lagally, M. G.; Celler, G. K.; Ma, Z. Flexible Photodetectors on Plastic Substrates by use of Printing Transferred Single-crystal Germanium Membranes. *Appl. Phys. Lett.* **2009**, *94*, 013102.

(14) Takei, K.; Takahashi, T.; Ho, J. C.; Ko, H.; Gillies, A. G.; Leu, P. W.; Fearing, R. S.; Javey, A. Nanowire Active-Matrix Circuitry for Low-Voltage Macroscale Artificial Skin. *Nat. Mater.* **2010**, *9*, 821−826.

(15) Wang, W.; Zhao, Q.; Li, H.; Wu, H.; Zou, D.; Yu, D. Transparent, Double-Sided, ITO-Free, Flexible Dye-Sensitized Solar Cells Based on Metal Wire/ZnO Nanowire Arrays. *Adv. Funct. Mater.* **2012**, *22*, 2775−2782.

(16) Changjoon, Y.; Gyoujin, C.; Sangsig, K. Electrical Characteristics of GaAs Nanowire-Based MESFETs on Flexible Plastics. *IEEE Trans. Electron Devices* **2011**, *58*, 1096−1101.

(17) Sun, Y.; Kim, H.-S.; Menard, E.; Kim, S.; Adesida, I.; Rogers, J. A. Printed Arrays of Aligned GaAs Wires for Flexible Transistors, Diodes, and Circuits on Plastic Substrates. *Small* **2006**, *2*, 1330−1334.

(18) Shin, G.; Bae, M. Y.; Lee, H. J.; Hong, S. K.; Yoon, C. H.; Zi, G.; Rogers, J. A.; Ha, J. S. SnO_2 Nanowire Logic Devices on Deformable Nonplanar Substrates. *ACS Nano* **2011**, *5*, 10009−10016.

(19) Ali Raza, S. R.; Hosseini Shokouh, S. H.; Lee, Y. T.; Ha, R.; Choi, H.-J.; Im, S. NiO_x Schottky-gated ZnO Nanowire Metal-Semiconductor Field Effect Transistor: Fast Logic Inverter and Photo-detector. *J. Mater. Chem. C* **2014**, *2*, 4428−4435.

(20) Dai, Y.; Yu, B.; Ye, Y.; Wu, P.; Meng, H.; Dai, L.; Qin, G. High-Performance CdSe Nanobelt Based MESFETs and Their Application in Photodetection. *J. Mater. Chem.* **2012**, *22*, 18442−18446.

(21) Blanchard, P. T.; Bertness, K. A.; Harvey, T. E.; Mansfield, L. M.; Sanders, A. W.; Sanford, N. A. MESFETs Made From Individual GaN Nanowires. *IEEE Trans. Nanotechnol.* **2008**, *7*, 760−765.

(22) Ye, Y.; Dai, L.; Wen, X.; Wu, P.; Pen, R.; Qin, G. High-Performance Single CdS Nanobelt Metal-Semiconductor Field-Effect Transistor-Based Photodetectors. *ACS Appl. Mater. Interfaces* **2010**, *2*, 2724−2727.

(23) Jin, W.; Gao, Z.; Zhou, Y.; Yu, B.; Zhang, H.; Peng, H.; Liu, Z.; Dai, L. Novel Graphene-Oxide-Semiconductor Nanowire Photo-transistors. *J. Mater. Chem. C* **2014**, *2*, 1592−1596.

(24) Jin, W.; Ye, Y.; Gan, L.; Yu, B.; Wu, P.; Dai, Y.; Meng, H.; Guo, X.; Dai, L. Self-Powered High Performance Photodetectors Based on CdSe Nanobelt/Graphene Schottky Junctions. *J. Mater. Chem.* **2012**, *22*, 2863−2867.

(25) Duan, X.; Niu, C.; Sahi, V.; Chen, J.; Parce, J. W.; Empedocles, S.; Goldman, J. L. High-Performance Thin-Film Transistors using Semiconductor Nanowires and Nanoribbons. *Nature* **2003**, *425*, 274−278.

(26) Wu, P.; Ye, Y.; Sun, T.; Peng, R.; Wen, X.; Xu, W.; Liu, C.; Dai, L. Ultrahigh-Performance Inverters Based on CdS Nanobelts. *ACS Nano* **2009**, *3*, 3138−3142.

(27) Yoon, C.; Moon, T.; Lee, M.; Cho, G.; Kim, S., Flexible Logic Gates Composed of High Performance GaAs-Nanowire-Based MESFETs with MHz-Dynamic Operations. *Nanotechnology* **2011**, *22*.

DOI: 10.1021/acsami.5b02929
ACS Appl. Mater. Interfaces 2015, 7, 13131−13136